2014

# Estimation of vegetation photosynthetic capacity from space-based measurements of chlorophyll fluorescence for terrestrial biosphere models

Yongguang Zhang
*Free University of Berlin*

Luis Guanter
*Free University of Berlin*

Joseph A. Berry
*Department of Global Ecology, Carnegie Institution for Science, Stanford, CA*

Joanna Joiner
*NASA Goddard Space Flight Center, Greenbelt, MD*

Christiaan van der Tol
*International Institute for Geo-Information Science and Earth Observation, P.O. Box 6, 7500 AA, Enschede, The Netherlands*

***See next page for additional authors***

Global Change Biology
celebrating 20 years

Global Change Biology (2014) **20**, 3727–3742, doi: 10.1111/gcb.12664

# Estimation of vegetation photosynthetic capacity from space-based measurements of chlorophyll fluorescence for terrestrial biosphere models

YONGGUANG ZHANG[1], LUIS GUANTER[1], JOSEPH A. BERRY[2], JOANNA JOINER[3], CHRISTIAAN VAN DER TOL[4], ALFREDO HUETE[5], ANATOLY GITELSON[6], MAXIMILIAN VOIGT[1] and PHILIPP KÖHLER[1]

[1]*Institute for Space Sciences, Free University of Berlin, Berlin 12165, Germany,* [2]*Department of Global Ecology, Carnegie Institution for Science, Stanford, CA 94305, USA,* [3]*NASA Goddard Space Flight Center, Greenbelt, MD 20771, USA,* [4]*International Institute for Geo-Information Science and Earth Observation, P.O. Box 6, 7500 AA, Enschede, The Netherlands,* [5]*Plant Functional Biology and Climate Change Cluster, University of Technology Sydney, Sydney, NSW 2007, Australia,* [6]*School of Natural Resources, University of Nebraska – Lincoln, Lincoln, NE 68583, USA*

## Abstract

Photosynthesis simulations by terrestrial biosphere models are usually based on the Farquhar's model, in which the maximum rate of carboxylation ($V_{cmax}$) is a key control parameter of photosynthetic capacity. Even though $V_{cmax}$ is known to vary substantially in space and time in response to environmental controls, it is typically parameterized in models with tabulated values associated to plant functional types. Remote sensing can be used to produce a spatially continuous and temporally resolved view on photosynthetic efficiency, but traditional vegetation observations based on spectral reflectance lack a direct link to plant photochemical processes. Alternatively, recent space-borne measurements of sun-induced chlorophyll fluorescence (SIF) can offer an observational constraint on photosynthesis simulations. Here, we show that top-of-canopy SIF measurements from space are sensitive to $V_{cmax}$ at the ecosystem level, and present an approach to invert $V_{cmax}$ from SIF data. We use the Soil-Canopy Observation of Photosynthesis and Energy (SCOPE) balance model to derive empirical relationships between seasonal $V_{cmax}$ and SIF which are used to solve the inverse problem. We evaluate our $V_{cmax}$ estimation method at six agricultural flux tower sites in the mid-western US using spaced-based SIF retrievals. Our $V_{cmax}$ estimates agree well with literature values for corn and soybean plants (average values of 37 and 101 μmol $m^{-2}$ $s^{-1}$, respectively) and show plausible seasonal patterns. The effect of the updated seasonally varying $V_{cmax}$ parameterization on simulated gross primary productivity (GPP) is tested by comparing to simulations with fixed $V_{cmax}$ values. Validation against flux tower observations demonstrate that simulations of GPP and light use efficiency improve significantly when our time-resolved $V_{cmax}$ estimates from SIF are used, with $R^2$ for GPP comparisons increasing from 0.85 to 0.93, and for light use efficiency from 0.44 to 0.83. Our results support the use of space-based SIF data as a proxy for photosynthetic capacity and suggest the potential for global, time-resolved estimates of $V_{cmax}$.

*Keywords:* Farquhar model Cropland, GPP, photosynthesis, SCOPE, Solar-induced fluorescence, $V_{cmax}$

*Received 11 March 2014; revised version received 9 June 2014 and accepted 11 June 2014*

## Introduction

Accurately quantifying global and regional terrestrial gross primary productivity (GPP) is considered of great importance due to its key role in the atmosphere-biosphere interactions. For several decades, state-of-the-art terrestrial biosphere models (TBM) have been used to quantify the variability of GPP at different temporal and spatial scales (Dickinson, 1983; Sellers *et al.*, 1997). Most of these models are based on C3 and C4 photosynthesis models developed by Farquhar *et al.* (1980) and Collatz *et al.* (1992) to calculate GPP, which are particularly sensitive to photosynthetic capacity, expressed as the maximum carboxylation capacity ($V_{cmax}$). $V_{cmax}$ is one of the key biochemical parameters in these photosynthesis models as it controls the carbon fixation process (Farquhar *et al.*, 1980). There are large spreads in GPP estimates in space and time across models (Schaefer *et al.*, 2012) owing to combinations of model structural error and parameter uncertainties (Bonan *et al.*, 2011). The latter case most notably relates to the uncertainty in $V_{cmax}$ that has a magnitude comparable to model structural errors with an offsetting sign (Bonan *et al.*, 2011). Thus, accurate estimations of $V_{cmax}$ are needed to simulate ecosystem GPP because

Correspondence: Yongguang Zhang, tel. +490 30 83859025, fax +490 30 83856664, e-mail: yongguang.zhang@wew.fu-berlin.de

potential bias or errors of $V_{cmax}$ may be exacerbated when upscaling from leaf to ecosystem level (Hanson *et al.*, 2004).

Despite its importance, large-scale estimates of $V_{cmax}$ remain challenging. As a leaf-level parameter, $V_{cmax}$ cannot be measured directly, but only be inferred indirectly from leaf-level measurements of gas exchange (Wullschleger, 1993). However, making such observations is labor-intensive and can only focus on measurements at leaf or plant scale. On the other hand, eddy covariance flux measurements together with meteorological observations provide another way to make ecosystem-level estimates of $V_{cmax}$ through inverse modeling from $CO_2$ and water fluxes (Wolf *et al.*, 2006; Wang *et al.*, 2007). However, the parameterization of $V_{cmax}$ in a global, spatially continuous and time-resolved manner remains an unsolved problem.

Several studies have recently shown that $V_{cmax}$ varies seasonally (Wilson *et al.*, 2001; Xu & Baldocchi, 2003; Grassi *et al.*, 2005), and that photoperiod may regulate seasonal patterns of photosynthetic capacity as shown by Bauerle *et al.* (2012), with $V_{cmax}$ approaching a maximum around the summer solstice and then declining synchronously with the photoperiod. However, only a few terrestrial biosphere models have incorporated such seasonal variations in photosynthetic capacity (Medvigy *et al.*, 2009; Oleson *et al.*, 2010). Most of the models either assume a constant $V_{cmax}$ over time or derive it from more easily measurable parameters (Grassi *et al.*, 2005) due to the limitations of available spatial and temporal information from relevant proxies. For example, in the widely used Community Land Model (CLM) (Oleson *et al.*, 2010) $V_{cmax}$ is assigned a specific value for each broadly defined plant functional type (PFT) and then adjusted with day length. There is increasing evidence that the assumption of time-invariant photosynthetic parameters can cause significant errors if large seasonal variability in photosynthetic capacity occurs (Wilson *et al.*, 2001; Kosugi *et al.*, 2003; Medvigy *et al.*, 2013). As a consequence, the broad implications of seasonal variations of $V_{cmax}$ on the carbon cycle are not well understood.

Remote sensing provides a unique opportunity to parameterize spatially explicit plant physiological information on local, regional and global scales, and thus improve simulations of carbon fluxes of terrestrial ecosystems (Hilker *et al.*, 2008). Many efforts have been made to estimate the functional attributes of plant canopies with remote sensing data. Classical reflectance-based vegetation indices (VI) (Tucker, 1979), such as Normalized Difference Vegetation Index (NDVI), have substantially improved our understanding of the global biosphere by providing estimates of potential photosynthesis from greenness estimates (Turner *et al.*, 2003; Running *et al.*, 2004). Some VIs like photochemical reflectance index (PRI) can be successfully used to derive light use efficiency (LUE) from multi-angle satellite data (Hilker *et al.*, 2011). However, reflectance-based measurements like NDVI are not directly linked to instantaneous photosynthetic processes and cannot alone quantify actual photosynthesis or its down-regulation due to environmental stresses. Therefore, the direct estimations of photosynthetic capacity ($V_{cmax}$) through space-based proxies have not yet been achieved.

As a complement to reflectance-based vegetation indices, solar-induced fluorescence (SIF) offers new possibilities to monitor photosynthesis from space (Baker, 2008). Solar-induced fluorescence is an electromagnetic emission in the 650–800 nm range originating at the core of the photosynthetic machinery. It has been used in leaf-scale studies of photosynthesis under laboratory conditions for several decades (Baker, 2008) and has also been shown to be an excellent proxy for GPP at canopy and ecosystem scales (Frankenberg *et al.*, 2011; Guanter *et al.*, 2012). Global data of SIF have recently been retrieved from a series of spaceborne instruments providing high resolution spectra, such as the GOSAT's Fourier Transform Spectrometer (Frankenberg *et al.*, 2011; Joiner *et al.*, 2011; Guanter *et al.*, 2012), ENVISAT/SCIAMACHY (Joiner *et al.*, 2012) and MetOp-A/GOME-2 (Joiner *et al.*, 2013). The new global retrievals of chlorophyll fluorescence enable the establishment of a direct link between a remotely sensed vegetation parameter related to photosynthetic capacity and actual terrestrial photosynthetic activity. In particular, the empirical study by Guanter *et al.* (2014) demonstrated that space-borne SIF is more sensitive to the high photosynthetic rates of cropland than other remotely sensed vegetation parameters.

In this work, we have used an integrated photosynthesis-fluorescence model, the Soil-Canopy Observation of Photochemistry and Energy fluxes (SCOPE) model, to invert $V_{cmax}$ from SIF retrievals obtained from GOME-2 data. Specifically, a key objective of this study is to investigate the utility of SIF as a proxy for photosynthetic capacity and to propose a new approach for spatially continuous and time-resolved estimation of $V_{cmax}$ from space-based SIF measurements.

## Materials and methods

### *SIF retrievals from GOME-2*

SIF (in radiance units) was derived from measurements by the GOME-2 instrument onboard Eumetsat's MetOp-A platform launched in October 2006. Details of the retrieval of SIF from GOME-2 measurements can be found in Joiner *et al.* (2013).

GOME-2 measures in the 240–790 nm spectral range with a spectral resolution between 0.2 and 0.5 nm and a nominal footprint of 40 × 80 $km^2$. SIF retrievals are based on the inversion of the top-of-atmosphere measurements in the 715–758 nm windows overlapping the second peak of the SIF emission. The retrieval method disentangles the contribution of atmospheric absorption and scattering, surface reflectance and fluorescence to the measured top-of-atmosphere radiance spectra. The retrievals are quality-filtered and binned in 0.5° latitude-longitude grid boxes (Joiner *et al.*, 2013). GOME-2 data between 2007 and 2011 have been used in this work. GOME-2 SIF retrievals were aggregated into biweekly periods to improve the signal-to-noise ratio of the SIF data.

### *Flux sites and data*

We used six crop flux tower sites located in the corn belt in the midwestern US (Table 1). Sites have been selected on the basis of landscape homogeneity within the GOME-2 grid and on data availability in the period of interest (2007–2011). To determine landscape homogeneity, we used the MODIS products for land cover type (MCD12C1, Friedl *et al.*, 2010), and Enhance Vegetation Index (EVI, MOD13C2, Huete *et al.*, 2002) with spatial resolution of 0.05 degree. We selected those sites for which more than 90% of the GOME-2 pixel area around the flux tower sites corresponds to croplands and EVI standard deviation is <0.10 (Table 1).

We obtained the Level 2 flux data products for the 6 US crop sites from the AmeriFlux website (http://ameriflux.ornl.gov/). Half-hourly or hourly data of $CO_2$ flux and associated meteorological variables were extracted. Gap-filling and flux-partitioning were all processed by the online tool available at http://www.bgc-jena.mpg.de/~MDIwork/eddyproc/from Max Planck Institute for Biogeochemistry (MPI-BGC). GPP was estimated by partitioning the observed net flux into GPP and ecosystem respiration as described in Reichstein *et al.* (2005) and Papale *et al.* (2006). Hourly absorbed photosynthetic active radiation (APAR) and fraction absorbed photosynthetic active radiation (FPAR) data was obtained from the flux data. Site-level leaf area index (LAI) and canopy height ($h_c$) measurements were available for each site every 2 weeks during the growing season.

For each site, SIF values were extracted based on the coordinates of the flux tower, and averaged to biweekly means when at least 5 SIF retrievals were available within each biweekly period. To avoid signal contamination from urban areas, we extracted SIF from nearby homogeneous pixels for those sites in which urban areas fell inside the GOME-2 pixel. Given that in homogeneous landscapes flux measurements are usually representative of a large area, (i.e., US-IB1 is representative of central Illinois), we assumed that SIF from nearby grid pixels can represent that at the flux sites. The SIF measurement error in each biweekly period is estimated as the standard error of the mean (SE) and a nominal constant error of 0.2 W $m^{-2}$ $\mu m^{-1}$ $sr^{-1}$ (Joiner *et al.*, 2013). The standard error alone appear to underestimate the uncertainties as the large numbers of samples used in the averaging process lead to relatively small standard errors. The constant error is introduced to account for other error sources such as cloud contamination and variability. We used the maximum values of the constant error and the standard error of the mean in each biweekly period.

### *The SCOPE model and input parameters*

SCOPE is a vertical (1-D) integrated radiative transfer and energy balance model (van der Tol *et al.*, 2009a). The model calculates radiation transport in a multilayer canopy as a function of the solar zenith angle and leaf orientation to simulate fluorescence in the observation direction. The biochemical component has recently been updated on Collatz *et al.* (1991, 1992) for C3 and C4 plants, respectively. It calculates the illumination and net radiation of leaves with respect to their position (distance from the top of canopy in units of leaf area) and orientation (leaf inclination and azimuth angle), and the spectra of reflected and emitted radiation as observed above the canopy in the specified satellite observation geometry. The spectral range (0.4–50 μm) includes the visible, near and shortwave infrared and the thermal domain, with respectively, 1, 1, 100 and 1000 nm resolution. The geometry of the vegetation is

**Table 1** Details about the study flux tower sites used in this study*

| Site ID | Latitude | Longitude | Study period | Max (LC) | MeanEVI | sdEVI | Crop rotations | References |
|---|---|---|---|---|---|---|---|---|
| USBo1 | 40.0062 | −88.2904 | 2007 | 98% | 0.5562 | 0.0399 | Corn | Ryu *et al.* (2011) |
| USIB1 | 41.8593 | −88.2227 | 2007–2008 | 98% | 0.4431 | 0.0780 | Corn at even years and soybean at odd years | Allison *et al.* (2004) |
| USNe1 | 41.1651 | −96.4766 | 2007–2011 | 95% | 0.5641 | 0.0627 | Continuous corn | Suyker *et al.* (2005) |
| USNe2 | 41.1649 | −96.4701 | 2007–2011 | 95% | 0.5608 | 0.0704 | Corn except in 2008 | Suyker *et al.* (2005) |
| USNe3 | 41.1797 | −96.4397 | 2007–2011 | 95% | 0.5731 | 0.0719 | Corn at odd years and soybean at even years | Suyker *et al.* (2005) |
| USRo1 | 44.7143 | −93.0898 | 2007–2010 | 98% | 0.4912 | 0.0953 | Corn at odd year and soybean at even year | |

*LC stands for Land Cover class; EVI is the MODIS Enhanced Vegetation Index; max(LC) stands for the percent of dominant vegetation cover within the GOME-2 pixel; sdEVI for standard deviation of EVI within the GOME-2 pixel.

treated in a stochastic way with 60 elementary layers, 13 discrete leaf zenith inclination and 36 leaf azimuth classes. The azimuthal distribution is uniform, while the zenith angle distribution is provided as input. It describes the sun-canopy-observer geometry and leaf orientation, so that the different biophysical processes for sunlit and shaded components can be considered. Radiative transfer of chlorophyll fluorescence is calculated using a module similar to the FluorSAIL model (Miller *et al*., 2005), but allowing leaf fluorescence to vary depending on position and orientation in the canopy. A leaf-level biochemical model calculates GPP, stomatal resistance, and the energy balance of the leaf together with fluorescence from the absorbed flux of PAR, canopy temperature, and ambient vapor, $CO_2$ and $O_2$ concentrations (van der Tol *et al*., 2009b). In a recent update, the stomatal conductance model in SCOPE has been replaced by that of Ball *et al.* (1991), and the relationship between photochemical and fluorescence yield is based on the Genty equation (Genty *et al*., 1989) and has been calibrated to observations from leaf-scale fluorescence and gas exchange experiments with C3 and C4 crops. The model calculates radiation transport in a multilayer canopy as a function of the solar zenith angle and leaf orientation to simulate fluorescence in the observation direction. Other significant updates were: the FLUSPECT module replaced PROSPECT model, the leaf-level biochemical model for fluorescence was changed, the within canopy gradient in $V_{cmax}$ parallels the extinction of light following Sellers *et al.* (1992), and the way of programming was changed by organizing variables in structures. In this work, we used the recent version of SCOPE (V. 1.52).

To simulate photosynthesis and fluorescence, SCOPE requires inputs of meteorological forcing (incoming shortwave and long-wave radiation, air temperature, humidity, wind speed, and $CO_2$ concentration) and four kinds of parameters: (1) *vegetation structure parameters*, such as canopy height, leaf size, leaf angle distribution, and LAI; (2) *leaf biophysical parameters*: leaf chlorophyll content($C_{ab}$), dry matter content($C_{dm}$), leaf equivalent water thickness ($C_w$), senescent material($C_s$), and leaf structure ($N$); (3) *optical parameters*: reflectance of soil in the visible, near infrared and thermal bands, and vegetation (thermal) emissivity; (4) *plant physiological parameters*: stomatal conductance parameter ($m$), and maximum carboxylation capacity, $V_{cmax}$ of a top leaf standardized to a reference temperature at 25 °C (parameter '$V_{cmo}$' in the model).

Meteorological inputs to constrain SCOPE were available from flux tower measurements. Values or sources of some other important input parameters required for the SCOPE model are listed in Table 2. Leaf angle distribution is assumed to be spherical, which is a good approximation in crops such as soybean and corn (Table 2) (Lemeur & Blad, 1974; Verhoef & Bach, 2007). Estimates of LAI and canopy height and their seasonal variations were derived from the AmeriFlux website. Based on soil texture classification from site-specific websites, soil reflectance spectra were derived from ASTER soil spectral library available at www.speclib.jpl.nasa.gov. Initial soil temperatures were set equal to the corresponding air temperatures.

$V_{cmax}$ is a key parameter for biochemical modeling of $CO_2$ assimilation in SCOPE. It is a leaf-scale photosynthetic parameter, assumed to decrease exponentially with the depth in a canopy. The parameter $V_{cmax}$ varies largely with different biomes (Wullschleger, 1993; Sellers *et al*., 1997), and with day of the year (Mäkelä *et al*., 2004). As stated in the objective of this study, this parameter was chosen to be inverted from SIF (section 'Inversion of $V_{cmax}$ during the growing season from SCOPE simulations and SIF data').

A rough estimation of $C_{ab}$, $C_w$, $C_{dm}$, and $N$ controlling the leaf and canopy radiative transfer was obtained from vegetation indices (VIs). Three VIs were used including NDVI and EVI (Huete *et al*., 2002), both extracted from the MOD13C2 product, and the MERIS terrestrial chlorophyll index (MTCI) (Dash & Curran, 2004). These indices provide indirect information on canopy structure and chlorophyll content. Many studies have shown the feasibility of inverting radiative transfer models using VIs to derive $C_{ab}$, $C_w$, $C_{dm}$, and $N$ (Jacquemoud *et al*., 1996; Combal *et al*., 2003; Maire *et al*., 2004). We

**Table 2** The input parameters used for SCOPE simulations

| Parameters | Symbol | Units | Range | Values or sources |
|---|---|---|---|---|
| Chlorophyll $a + b$ content | $C_{ab}$ | μg cm$^{-2}$ | 10–70 | Inverted from VIs |
| Dry matter content | $C_{dm}$ | g cm$^{-2}$ | 0.001–0.02 | Inverted from VIs |
| Leaf equivalent water thickness | $C_w$ | cm | 0.001–0.05 | Inverted from VIs |
| Senescent material | $C_s$ | / | / | 0.0 |
| Leaf structure | N | / | 1.3–2.0 | Inverted from VIs |
| Leaf angle distribution parameter $a$ | LIDF$_a$ | / | / | −0.35 |
| Leaf angle distribution parameter $b$ | LIDF$_b$ | / | / | −0.15 |
| Leaf width | $w$ | m | / | 0.1 |
| Ball-Berry stomatal conductance parameter | $m$ | / | / | Corn: 4; Soybean: 9 |
| Dark respiration rate at 25 °C as fraction of $V_{cmax}$ | $R_d$ | / | / | 0.015 |
| Cowan's water use efficiency parameter | $\lambda_c$ | | | 700 |
| Leaf thermal reflectance | $\rho$ (thermal) | / | / | 0.01 |
| Leaf thermal transmittance | $\tau$ (thermal) | / | / | 0.01 |
| Soil thermal reflectance | $\rho_s$ (thermal) | / | / | 0.06 |
| Leaf area index | LAI | / | / | Field measurement |
| Canopy height | $h_c$ | m | / | Field measurement |

use a look-up table approach to solve the inversion problem which requires less computing time and generally performs well. The leaf reflectance model PROSPECT (Jacquemoud & Baret, 1990) was used for the inversion, which was also integrated into the SCOPE model. We built a database composed of hundreds of thousands of simulated leaf reflectance spectra with the PROSPECT model with a 1 nm resolution in forward mode. The ranges of the $C_{ab}$, $C_w$, $C_{dm}$, and $N$ parameters are chosen from observed data (the LOPEX data set, Hosgood *et al*., 1994). The values of each parameter are given in Table 2. The space of model input variables was sampled by randomly drawing values by assuming uniform distribution function of each variable. The generated database contains a total of 280 000 simulations representing a wide range of leaves. A simple cost function was used to find the solution to the inverse problem, which minimizes the root mean squared error (RMSE) between measured and simulated vegetation indices. Monthly VIs were extracted based on the coordinates of the flux tower. To avoid an ill-posed problem we used the median from the best 100 simulations (Combal *et al*., 2003; Darvishzadeh *et al*., 2008). We also checked the use of median of the best 10, 20, and 40 simulations and found no significant differences (data not shown). The resulting seasonal variables of $C_{ab}$, $C_w$, $C_{dm}$, and $N$ were used as input biophysical parameters for SCOPE at each site.

### *Inversion of $V_{cmax}$ during the growing season from SCOPE simulations and SIF data*

A schematic diagram of SIF-based $V_{cmax}$ retrieval scheme is given in Fig. 1. With the meteorological and other input parameters stated above, SCOPE was first run with a LUT of $V_{cmax}$ at half-hourly or hourly time steps at the flux tower sites for the 2007–2011 period. Based on the published literature (Wullschleger, 1993; Kattge *et al*., 2009; Lokupitiya *et al*., 2009), the ranges of $V_{cmax}$ were set to 10–70 μmol $m^{-2}$ $s^{-1}$ with a step of 5 μmol $m^{-2}$ $s^{-1}$ for corn and 10–200 μmol $m^{-2}$ $s^{-1}$ with a step 10 μmol $m^{-2}$ $s^{-1}$ for soybean, respectively. We also tested a smaller step; this showed no significant differences (data not shown), but had a higher computational cost. We also used a bigger LUT of $V_{cmax}$ (up to 320 and 120 μmol $m^{-2}$ $s^{-1}$ for soybean and corn, respectively) and found that the linear relationship became non-linear after around 200 and 70 μmol $m^{-2}$ $s^{-1}$ for soybean and corn, respectively. This means that $V_{cmax}$ become non-limiting at ambient light and simulated chlorophyll fluorescence did not increase with $V_{cmax}$ at higher values.

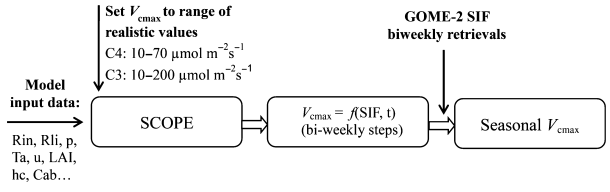


**Fig. 1** Overview flowchart of the Soil-Canopy Observation of Photosynthesis and Energy simulations and inversions of $V_{cmax}$ from solar-induced fluorescence.

Relationships between $V_{cmax}$ and canopy fluorescence were established by running the SCOPE model in forward mode. The relationships were derived separately for different vegetative growth periods during the growing season for each year and each site as shown in the section 'Relationship between $V_{cmax}$ and SIF during the growing season from SCOPE simulations'. To match the biweekly GOME-2 SIF retrievals, we derived the relationship for each biweekly period during the growing season. This implies that for each biweekly period, a unique linear relationship was established for the inverse retrieval of $V_{cmax}$ from GOME-2 SIF at each site. Then, using corresponding GOME-2 SIF biweekly retrievals, seasonal $V_{cmax}$ was inverted from the derived relationships for corn and soybean during the growing season for each year and each site, respectively. We estimated the uncertainties in each biweekly period from the measurement error of SIF which was propagated to $V_{cmax}$ through the linear models between $V_{cmax}$ and SIF.

It should be noted that, due to the coarse resolution of GOME-2, we applied this inversion approach on a mixture of corn and soybean canopies assuming similar intrinsic light use efficiency of fluorescence and a similar intrinsic FPAR for them. Although FPAR and the canopy light use efficiency of fluorescence vary with chlorophyll content $C_{ab}$ and leaf area (Gitelson *et al*., 2012), the intrinsic light use efficiency of fluorescence at photosystem level is assumed to be equal for both crops. This means that the two crops produce similar canopy fluorescence and electron transport rates (ETR) (Weis & Berry, 1987; Genty *et al*., 1989; Baker, 2008). Actual ETR is similar (Fig. 2) for soybean and corn despite large differences in their rates of $CO_2$ assimilation related to the difference in photosynthetic pathways. In Fig. 2, actual ETR for corn and soybean was calculated according to von Caemmerer & Farquhar (1981) from $CO_2$ assimilation rate (GPP) estimated from flux tower measurements for the year 2007 (corn, C4) and 2008 (soybean, C3) at the site of US-Ne3. We compare the daily cycles of actual ETR for the peak month for corn (July) and soybean (August), respectively. The mean ratio of ETR corn/soybean is 1.09 (±0.12) from flux tower measurements. This comparison demonstrates the similar actual ETR of these two crops which supports our assumption that the two crops produce similar canopy fluorescence. Previous work (Edwards & Baker, 1993) showed that the coupling of fluorescence to ETR is similar for C3 and C4 species. We conclude that while the area is a mixture of soybean and corn, we can use the observed fluorescence properties of the mixture as if it were all soybean or all corn and solve for the respective values of $V_{cmax}$ that are consistent with the observations.

After the $V_{cmax}$ inversion, we performed time-series simulations of GPP and canopy fluorescence at half-hourly or hourly steps using SCOPE with parameters stated above (Table 2) for each site. SCOPE was run with two different configurations to evaluate the effect of $V_{cmax}$ parameterizations on simulated SIF and GPP. The following SCOPE simulations were conducted:

1. Fixed $V_{cmax}$: simulations with a constant PFT-specific $V_{cmax}$ values: 54 μmol $m^{-2}$ $s^{-1}$ for corn, and 100 μmol $m^{-2}$ $s^{-1}$ for soybean (Wullschleger, 1993; Kattge *et al*., 2009;

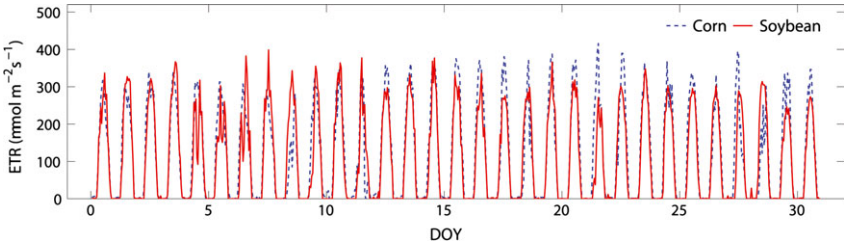


**Fig. 2** A comparison of daily cycles of calculated actual electron transport rate for the peak month of corn and soybean with $CO_2$ assimilation rate estimated from flux tower measurements gross primary productivity. The month is July for corn, and August for soybean (see main text for detail).

Lokupitiya *et al.*, 2009) which are commonly used in the TBM community.

2. $V_{cmax}$ = *f*(SIF): simulations with $V_{cmax}$ as a function of SIF from GOME-2 retrievals. For seasonal $V_{cmax}$, we used an arbitrary value of 10 μmol $m^{-2}$ $s^{-1}$ for the non-growing season periods.

### *Analysis of SCOPE simulations with different $V_{cmax}$ configurations*

GOME-2 has a sun-synchronous orbit and samples near 9:30 hours local time. We used data only under mostly clear-sky condition up to cloud fraction of 40% or less. From SCOPE model results, we defined midday values of fluorescence as average values between 09:00 and 12:00 hours. To match the window of inversion of GOME-2 SIF, we determined the model values of fluorescence of that at the 740 nm wavelengths. We also integrated the half-hourly or hourly simulations to biweekly to compare with GOME-2 SIF retrievals. For GPP, we used the average of 24-hour values of each day for both flux tower estimates and model results, and then aggregated to biweekly values for comparisons. The results of GPP generated from the SCOPE model were similarly aggregated and validated against flux tower observations at each site. To show the feasibility of modeling SIF with SCOPE, we compared the SIF simulations with PFT-fixed $V_{cmax}$ with GOME-2 SIF retrievals. Due to the spatial mismatch between GOME-2 grid cell and flux tower footprint, we also compared the SIF simulations with seasonal variable $V_{cmax}$ with satellite retrievals for corn and soybean to validate our inversion process. In addition to SIF and GPP comparisons with different $V_{cmax}$ parameterizations, we also compared the two light use efficiencies: $LUE_p$ and $LUE_f$. $LUE_p$ represents photosynthetic light use efficiency, defined as GPP/APAR. $LUE_f$ represents light use efficiency for SIF (i.e., the fraction of absorbed PAR photons that are re-emitted from the canopy as SIF photons); this is also known as fluorescence quantum yield (Govindjee, 2004), and is obtained by dividing SIF by APAR.

The performance of inversions of $V_{cmax}$ from SIF was evaluated against the data by different validation statistics including the mean absolute error (MAE) and the root mean squared error (RMSE):

$$\mathrm{MAE} = \frac{1}{n}\sum_{i=1}^{n} \mathrm{abs}(\mathrm{RES}_i)$$

$$\mathrm{RMSE} = \sqrt{\frac{1}{n}\sum_{i=1}^{n} \mathrm{RES}_i^2}$$

$RES_i$ denotes the residual at the *i*th observations, i.e., $OBS_i$–$SIM_i$, where $OBS_i$ and $SIM_i$ are the corresponding observed and simulated values.

## Results

### *Relationship between $V_{cmax}$ and SIF during the growing season from SCOPE simulations*

SCOPE simulations have shown strong linear relationships between $V_{cmax}$ and canopy fluorescence at biweekly steps during the growing season for corn and soybean, respectively (Fig. 3). Figure 3 illustrates these relationships for one example (the site of US-Ne3 at Mead, Nebraska in 2007 and 2008). This site has the longest period of data after 2007 and longest rotations of corn and soybean (Table 1). The top panel is for soybean in 2008, and the bottom is for corn in 2007. The other years and sites had similar patterns so they are not shown. Chlorophyll fluorescence increased linearly with $V_{cmax}$ within the range of our look-up tables. This suggests that $V_{cmax}$ has a significantly positive impact on simulations of SIF when other parameters, such as radiation, LAI, and Cab, remain unchanged using ancillary observations.

The slope of the linear relationship between $V_{cmax}$ and SIF varies for different biweekly periods (Fig. 3). The variations were substantial between the mid-growing season and early or end of the growing season. The slopes of fits between $V_{cmax}$ and SIF decreased from start to the mid-growing season, and then increased to the end of the growing season (Fig. 3b, d).The reason for such seasonal shifts may be due to seasonal variations of APAR. Figure 3a, d show that the slopes of fits have significantly negative correlation with APAR for both corn and soybean (Pearson correlation, $r > 0.9$,

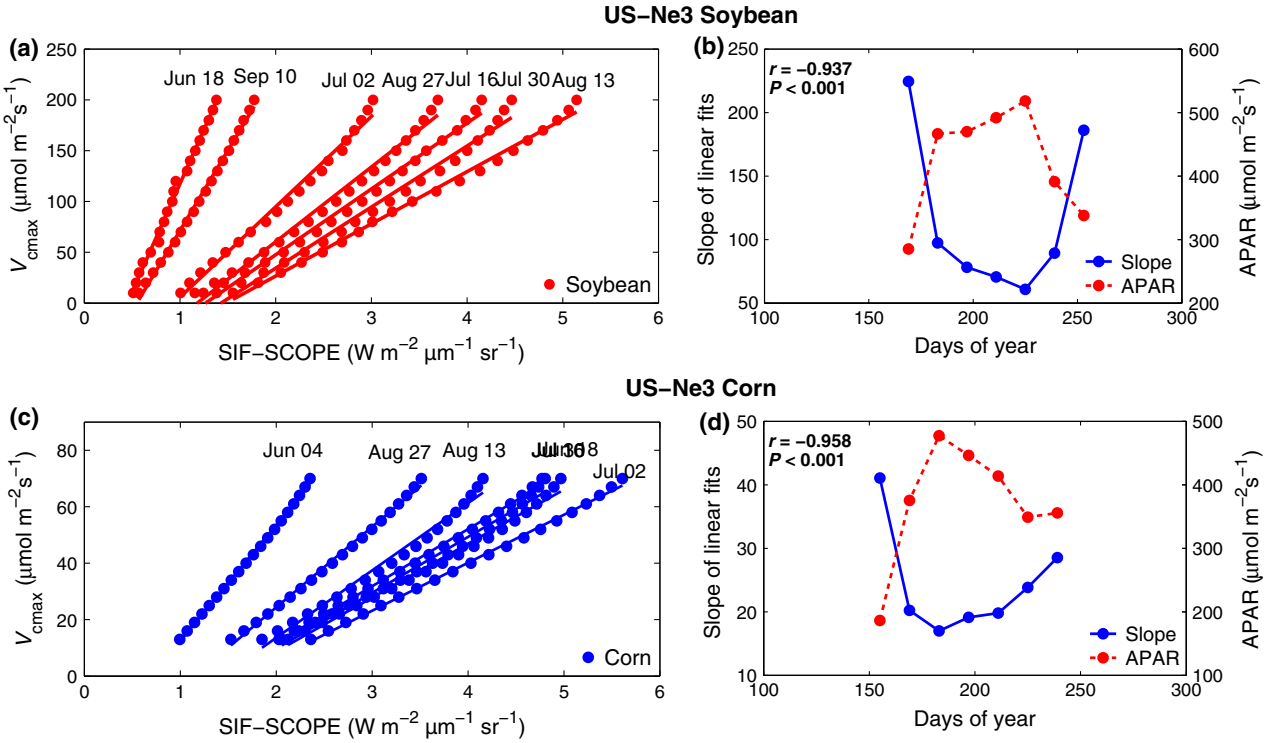


**Fig. 3** Relationship between biweekly $V_{cmax}$ and solar-induced fluorescence from Soil-Canopy Observation of Photosynthesis and Energy simulations for soybean (a) and corn (c) years at the US Ne3 site. (b) and (d) are the slopes of the fits in (a) and (c) and the seasonal absorbed photosynthetic active radiation (APAR) during the growing season. Pearson product–moment correlations are shown between the slopes and APAR in (b) and (d). Each linear relationship represents a biweekly period during the growing season, e.g., the first left most line in (a) is for June 18–July 1 of 2008.

$P < 0.001$). In addition, the slopes are rather high in the very early or end of the growing season (e.g., June 18 for soybean in Fig. 3a, b), implying that larger increases in $V_{cmax}$ would only result in smaller increases in canopy SIF and that plant carboxylation rates may not be Rubisco-limited and $V_{cmax}$ may be non-limiting during this period. However, much more work is needed in the future to investigate this underlying mechanism of growing season shifts between $V_{cmax}$ and SIF. In this study, we focused on the utilization of this linear relationship to retrieve $V_{cmax}$ from space measurements of GOME-2.

### *Seasonal variability of $V_{cmax}$ from SIF*

With the derived linear relationships shown above, seasonal values of $V_{cmax}$ were retrieved using the GOME-2 biweekly retrievals for each year and each site. Figure 4 shows the temporal evolution of $V_{cmax}$ and its uncertainties derived from SIF over the growing season for all the six sites during 2007–2011. The values of $V_{cmax}$ for soybean are higher than those for corn and both are in good agreement with published values (Wullschleger, 1993). During the growing season, our estimates for $V_{cmax}$ of corn at 25 °C varied from 11 to 75 μmol m$^{-2}$ s$^{-1}$ with an average of 37 μmol m$^{-2}$ s$^{-1}$ for all the years and sites, while the soybean $V_{cmax}$ ranged from 17 to 190 μmol m$^{-2}$ s$^{-1}$ with an average 101 μmol m$^{-2}$ s$^{-1}$. The uncertainties of $V_{cmax}$ due to the uncertainties in SIF are approximately 4.3 ± 1.2 and 10.9 ± 4.4 μmol m$^{-2}$ s$^{-1}$ for corn and soybean, or approximately 13.2 ± 6.5% of mean $V_{cmax}$ for corn and 12.3 ± 6.3% of mean $V_{cmax}$ for soybean for all site-years together (Fig. 4).

As expected, there were strong seasonal variations in $V_{cmax}$ (Fig. 4). During the growing season, $V_{cmax}$ increased rapidly with time and reached maximum values at early-mid-growing season for all the years and sites except the year 2007 at the Mead site (US Ne1-3) which had peak values in later growing season of late July or early August. Thereafter, there was a rapid decline in $V_{cmax}$ toward the end of the growing season as leaves started to senesce. Due to different planting dates and lengths of growing season for corn and soybean, $V_{cmax}$ generally peaked later for soybean than for corn (Fig. 4). This suggests that both the timing and amplitude of the seasonally varying $V_{cmax}$ was associated with the onset of leaf growth difference between the two crops.

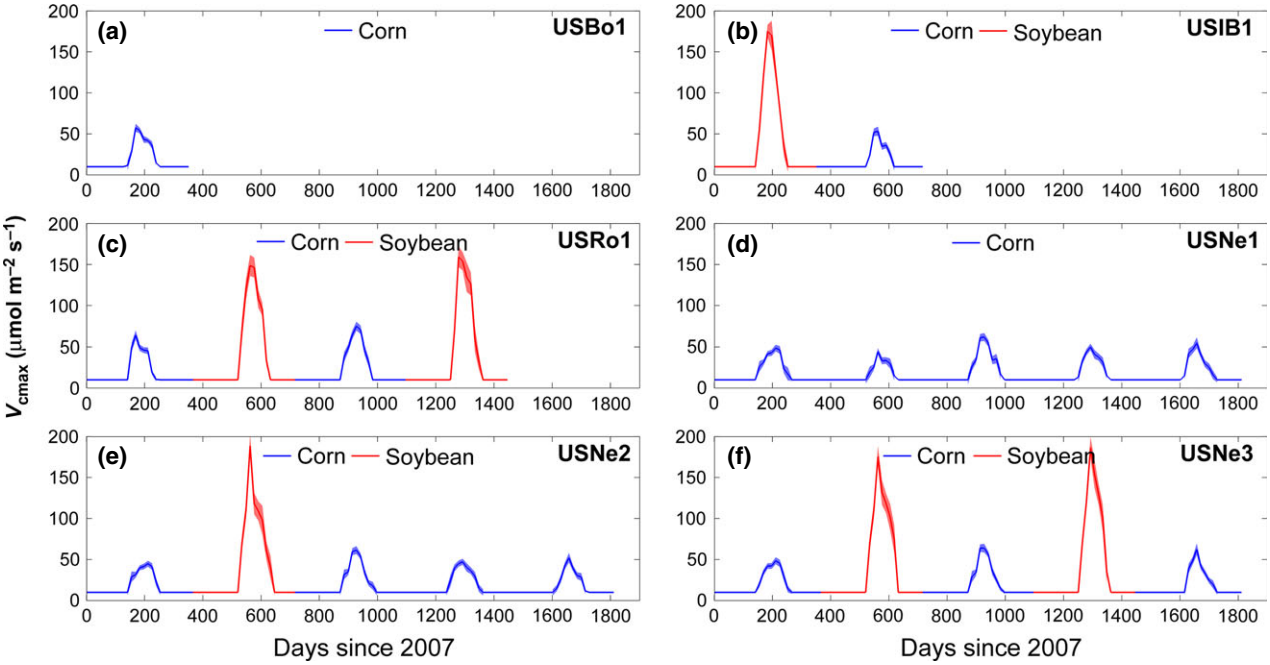


**Fig. 4** Seasonal variability of $V_{cmax}$ at 25 °C inverted from GOME-2 solar-induced fluorescence retrievals for six crop flux sites at biweekly step during 2007–2011. (a)USBo1, (b)USIB1,(c)USRo1,(d)USNe1,(e)USNe2, and (f)USNe3. See Table 1 for site information. Greyed areas indicate estimated uncertainties as discussed in the text.

### *SIF simulations with different $V_{cmax}$ parameterizations*

Here, for the first time, we evaluate SCOPE SIF simulations with GOME-2 space retrievals. To show that the inversion scheme is working properly, we compared the SIF simulations with constant and seasonally varying $V_{cmax}$ parameterizations. As an example, Fig. 5 demonstrates the seasonal impact of using different $V_{cmax}$ parameterizations on modeled canopy fluorescence for the crop flux site of US Ne3 at Mead, Nebraska. Figure 5a compares the biweekly time-series of GOME-2 SIF retrievals with its standard error to SCOPE simulations using a fixed $V_{cmax}$ of 54 and 100 μmol m$^{-2}$ s$^{-1}$ for corn and soybean, respectively, and $V_{cmax}$ derived from biweekly GOME-2 SIF time-series record. Figure 5b, c show the same data as scatter plots. Figure 6 present this comparison between observed and modeled SIF for all site-years together. Table 3 lists the $R^2$ values and bias error between observations and model predictions for each of the sites. Generally, there are good agreements between model predictions and measurements for both simulations and we also observe an improvement in the SIF simulations when seasonal $V_{cmax}$ is used. Figure 5 also shows that there are similar canopy SIF for corn and soybean from SCOPE simulations. The similar SIF simulations from SCOPE again prove our assumption of similar fluorescence yield for both crops even though they have different photosynthesis rate (or GPP, Gitelson *et al.*, 2012). In these simulations, the results from seasonally varying $V_{cmax}$ generally tracked the observations a little more closely, especially for soybean. The use of seasonal $V_{cmax}$ reduces bias error (MAE from 0.59 to 0.36 μmol m$^{-2}$ s$^{-1}$, Fig. 6) and the correlation coefficient ($R^2$) increases from 0.80 to 0.88. However, some high values of SIF were not captured by either type of simulation (Fig. 5). In addition, the model was unable to simulate the earlier onset (late May and early June) of crop growth for soybean in years 2008 and 2010 (Fig. 5a). This is possibly due to the spatial mismatch between GOME-2 and the flux tower footprint. Obviously, GOME-2 pixels contain more than one crop, resulting in what is often referred to as mixed pixels. There was a much greater portion of corn crop area within the GOME-2 pixels than soybean area, and soybean is usually planted later (USDA, 2010; USDA National Agricultural Statistics Service Cropland Data Layer, 2013).

### *GPP simulations with different $V_{cmax}$ parameterizations*

We compare flux tower-based GPP estimates with SCOPE simulations. We first present the comparisons on an hourly time scale for an example site. Figure 7 compares predicted and observed hourly values of GPP for the US Ne3 site during the period of 2007–2011. Generally, hourly GPP is substantially overestimated for corn and underestimated for soybean when a constant $V_{cmax}$ is assumed (Fig. 7a). Clearly, the use of $V_{cmax}$ as a function of biweekly GOME-2 SIF improved

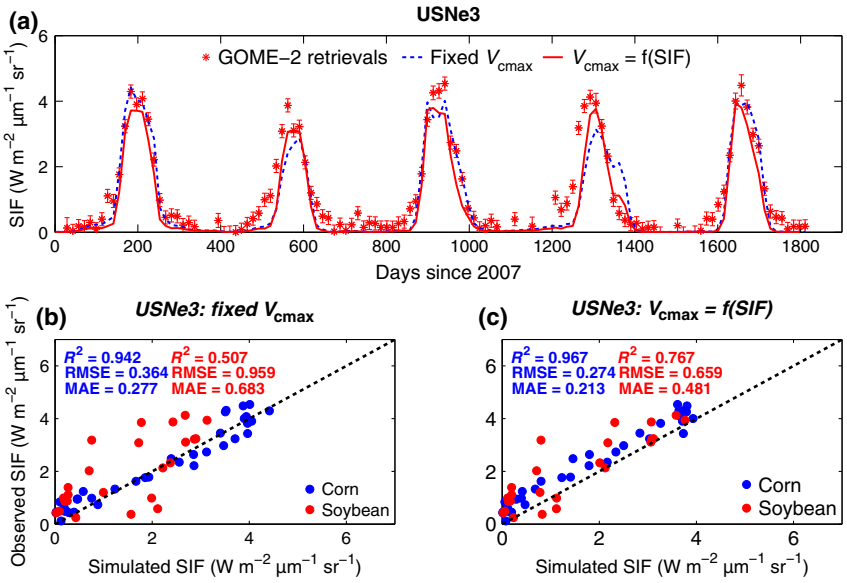


**Fig. 5** Site US-Ne3, (a) Seasonal comparison of solar-induced fluorescence (SIF) from GOME-2 retrievals against Soil-Canopy Observation of Photosynthesis and Energy (SCOPE) simulations at biweekly step using constant (dot line) and seasonal variable (solid line) $V_{cmax}$. Soybean is in 2008 and 2010; corn for other years. (b) Scatter plots of SIF between GOME-2 retrievals and SCOPE simulations with constant $V_{cmax}$. (c) Scatter plots of SIF between GOME-2 retrievals and SCOPE simulations with seasonal variable $V_{cmax}$ inverted from GOME-2 retrievals.

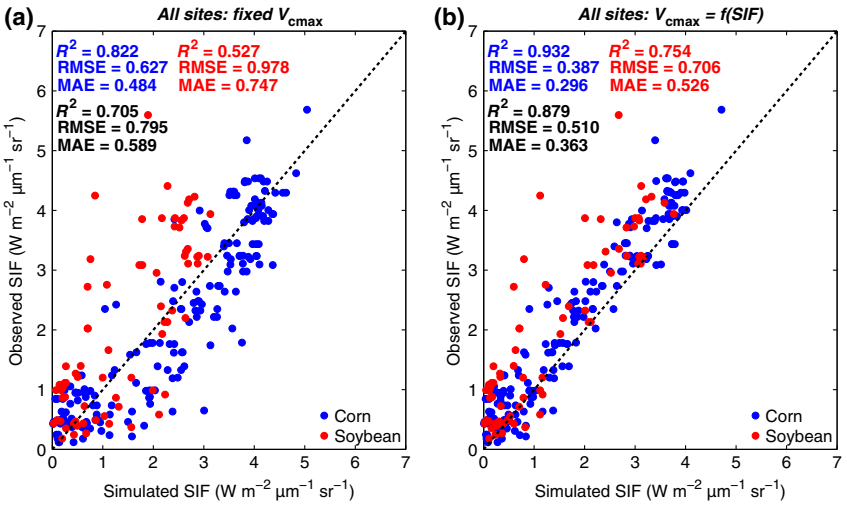


**Fig. 6** Scatter plots of GOME-2 solar-induced fluorescence retrievals against Soil-Canopy Observation of Photosynthesis and Energy simulations at biweekly step using (a) constant $V_{cmax}$ and (b) seasonal variable $V_{cmax}$ for all site-years at biweekly step during 2007–2011.

hourly GPP modeling, which is evidenced by an increase of the correlation coefficient ($R^2$) from 0.82 to 0.92 and a reduction of bias error (MAE) from 6.1 to 4.0 μmol m$^{-2}$ s$^{-1}$ (Fig. 7b). The simulations underestimate high GPP values for soybean, but the underestimation is substantially reduced with seasonal $V_{cmax}$ (Fig. 7b). The results for other sites show similar improvements in GPP modeling with seasonally varying $V_{cmax}$ from SIF.

On a seasonal time scale, the use of seasonal variable $V_{cmax}$ also improves the correlation between observed and modeled values for biweekly GPP and reduces the bias, especially for soybean. The overall performance of the seasonal impact of using different $V_{cmax}$ parameterizations on modeled bi-weekly GPP for all site-years is presented in Figs 8 and 9; Table 3. The time-series of modeled and observed GPP shows that the SCOPE model can track the seasonal variability of

**Table 3** Model-observed data comparisons statistics for biweekly SIF, GPP, $LUE_p$ and $LUE_f$ at the six sites*

| | | Fixed $V_{cmax}$ | | | | | | $V_{cmax} = f$(SIF) | | | | | |
|---|---|---|---|---|---|---|---|---|---|---|---|---|---|
| | Statistic | USBo1 | USIB1 | USNe1 | USNe2 | USNe3 | USRo1 | USBo1 | USIB1 | USNe1 | USNe2 | USNe3 | USRo1 |
| SIF-C3 | $R^2$ | | 0.555 | 0.873 | | 0.810 | 0.699 | | 0.804 | 0.927 | | 0.882 | 0.836 |
| | RMSE | | 1.174 | 0.499 | | 0.537 | 0.737 | | 0.779 | 0.378 | | 0.422 | 0.544 |
| | MAE | | 0.698 | 0.378 | | 0.400 | 0.500 | | 0.479 | 0.277 | | 0.291 | 0.379 |
| SIF-C4 | $R^2$ | 0.815 | 0.827 | 0.856 | 0.903 | 0.925 | 0.954 | 0.946 | 0.911 | 0.949 | 0.957 | 0.961 | 0.957 |
| | RMSE | 0.808 | 0.590 | 0.560 | 0.438 | 0.400 | 0.315 | 0.441 | 0.424 | 0.333 | 0.291 | 0.288 | 0.305 |
| | MAE | 0.730 | 0.416 | 0.368 | 0.308 | 0.209 | 0.226 | 0.287 | 0.300 | 0.241 | 0.209 | 0.208 | 0.221 |
| GPP-C3 | $R^2$ | | 0.712 | 0.869 | | 0.945 | 0.898 | | 0.980 | 0.936 | | 0.964 | 0.978 |
| | RMSE | | 2.415 | 1.410 | | 1.005 | 1.597 | | 0.640 | 0.990 | | 0.813 | 0.739 |
| | MAE | | 2.031 | 0.723 | | 0.620 | 0.689 | | 0.372 | 0.500 | | 0.355 | 0.419 |
| GPP-C4 | $R^2$ | 0.752 | 0.976 | 0.865 | 0.960 | 0.945 | 0.969 | 0.904 | 0.950 | 0.953 | 0.986 | 0.977 | 0.987 |
| | RMSE | 2.788 | 1.005 | 2.353 | 1.518 | 1.789 | 1.282 | 1.732 | 1.447 | 1.387 | 0.890 | 1.169 | 0.826 |
| | MAE | 2.051 | 0.675 | 1.322 | 0.904 | 1.020 | 0.788 | 1.172 | 0.795 | 0.798 | 0.495 | 0.603 | 0.447 |
| $LUE_p$-C3 | $R^2$ | | 0.591 | 0.552 | | 0.421 | 0.485 | | 0.619 | 0.836 | | 0.809 | 0.647 |
| | RMSE | | 0.704 | 0.381 | | 0.612 | 0.776 | | 0.635 | 0.396 | | 0.351 | 0.642 |
| | MAE | | 0.457 | 0.305 | | 0.464 | 0.585 | | 0.486 | 0.295 | | 0.252 | 0.499 |
| $LUE_p$-C4 | $R^2$ | 0.294 | 0.373 | 0.236 | 0.515 | 0.694 | 0.790 | 0.939 | 0.543 | 0.761 | 0.773 | 0.939 | 0.963 |
| | RMSE | 0.578 | 0.988 | 1.213 | 0.625 | 0.743 | 0.789 | 0.170 | 0.444 | 0.678 | 0.427 | 0.332 | 0.332 |
| | MAE | 0.424 | 0.660 | 0.924 | 0.471 | 0.555 | 0.583 | 0.128 | 0.727 | 0.474 | 0.283 | 0.258 | 0.241 |
| $LUE_f$-C3 | $R^2$ | | 0.426 | 0.570 | | 0.408 | 0.000 | | 0.686 | 0.932 | | 0.779 | 0.687 |
| | RMSE | | 0.253 | 0.148 | | 0.347 | 0.284 | | 0.187 | 0.062 | | 0.212 | 0.235 |
| | MAE | | 0.181 | 0.112 | | 0.234 | 0.200 | | 0.114 | 0.044 | | 0.148 | 0.130 |
| $LUE_f$-C3 | $R^2$ | 0.465 | 0.560 | 0.151 | 0.089 | 0.003 | 0.073 | 0.852 | 0.287 | 0.728 | 0.723 | 0.834 | 0.854 |
| | RMSE | 0.165 | 0.104 | 0.237 | 0.173 | 0.242 | 0.264 | 0.087 | 0.087 | 0.134 | 0.096 | 0.099 | 0.105 |
| | MAE | 0.115 | 0.071 | 0.162 | 0.126 | 0.063 | 0.201 | 0.058 | 0.058 | 0.089 | 0.063 | 0.053 | 0.079 |

*$LUE_p$ represent photosynthesis light use efficiency; $LUE_f$ represent light use efficiency for SIF which is fluorescence yield (i.e. the fraction of absorbed PAR photons that are re-emitted from the canopy as SIF photons); RMSE, root mean squared error; MAE, mean absolute error.

photosynthesis fairly well with both constant and seasonally varying $V_{cmax}$ (Fig. 8). However, SCOPE generally overestimates GPP for corn during the mid-late growing season, and underestimates GPP for soybean during the mid-growing season when a fixed $V_{cmax}$ is used (Fig. 8). When the seasonality of $V_{cmax}$ inverted from SIF is incorporated into the model, SCOPE more accurately simulates the seasonal variations of GPP (Fig. 8), with $R^2$ values >0.94 for all the sites (Table 3), and a reduction of bias by more than 40% for all sites together (Fig. 9). For example, the mid-late growing season GPP is better captured for corn for all the site-years (Fig. 8). The regression of observed vs. modeled GPP is closer to the 1 : 1 line with seasonally varying $V_{cmax}$ with slopes between 0.95 and 1.08 for corn and soybean, respectively (Fig. 9).

### *Light use efficiency of photosynthesis ($LUE_p$) and fluorescence yield ($LUE_f$) with different $V_{cmax}$ parameterizations*

To further evaluate the performance of our derived seasonally varying $V_{cmax}$ from GOME-2 data and also to evaluate its effect on photosynthesis modeling, we compare flux tower data with simulations of the canopy-level light use efficiency of photosynthesis ($LUE_p$) and fluorescence yield ($LUE_f$) before and after implementing retrieved seasonal $V_{cmax}$. Figures 10 and 11 show the comparisons of simulated $LUE_p$ and $LUE_f$ from constant and seasonal $V_{cmax}$ for all site-years together, while Table 3 lists some statistical information ($R^2$, RMSE and MAE) for corn and soybean for each of the sites. It should be noted that we only calculate daytime $LUE_p$ and $LUE_f$ during the growing season because of unrealistic values during night and the non-growing season. We observe that modeling $V_{cmax}$ as a function of SIF improved the simulations of $LUE_p$ and $LUE_f$ as compared with constant $V_{cmax}$ parameterizations, providing a closer match with observations during the growing season (Figs 10 and 11; Table 3). The correlation coefficient ($R^2$) increases from 0.44 to 0.83, and the bias (MAE) is reduced from 0.75 to 0.40 for $LUE_p$ for all sites together (Fig. 11). For $LUE_f$, the improvement is much larger with an increase of $R^2$ from 0.1 to 0.73, and a reduction of bias error (MAE) from 0.18 to 0.10 (Fig. 10). With constant $V_{cmax}$, there

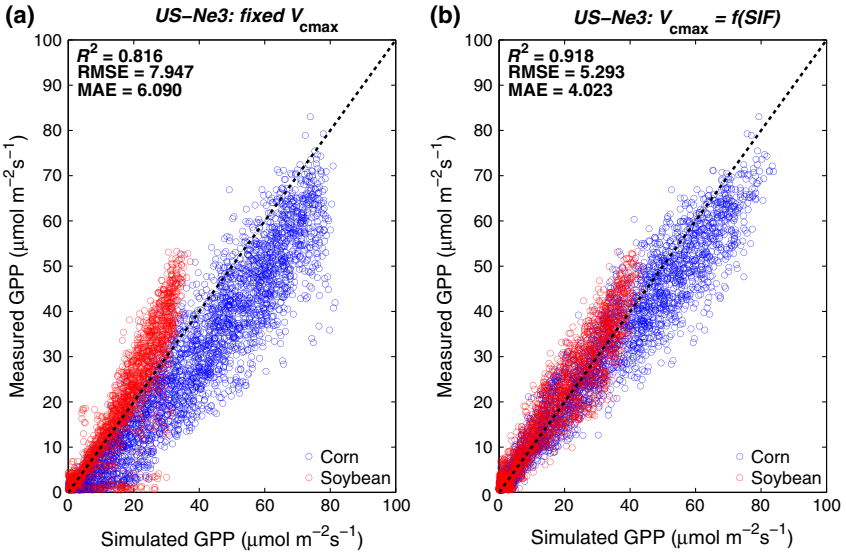


**Fig. 7** Scatter plots of flux tower estimated hourly gross primary productivity against Soil-Canopy Observation of Photosynthesis and Energy simulations with (a) fixed $V_{cmax}$ and (b) seasonal variable $V_{cmax}$ during 2007–2011 at USNe3 site.

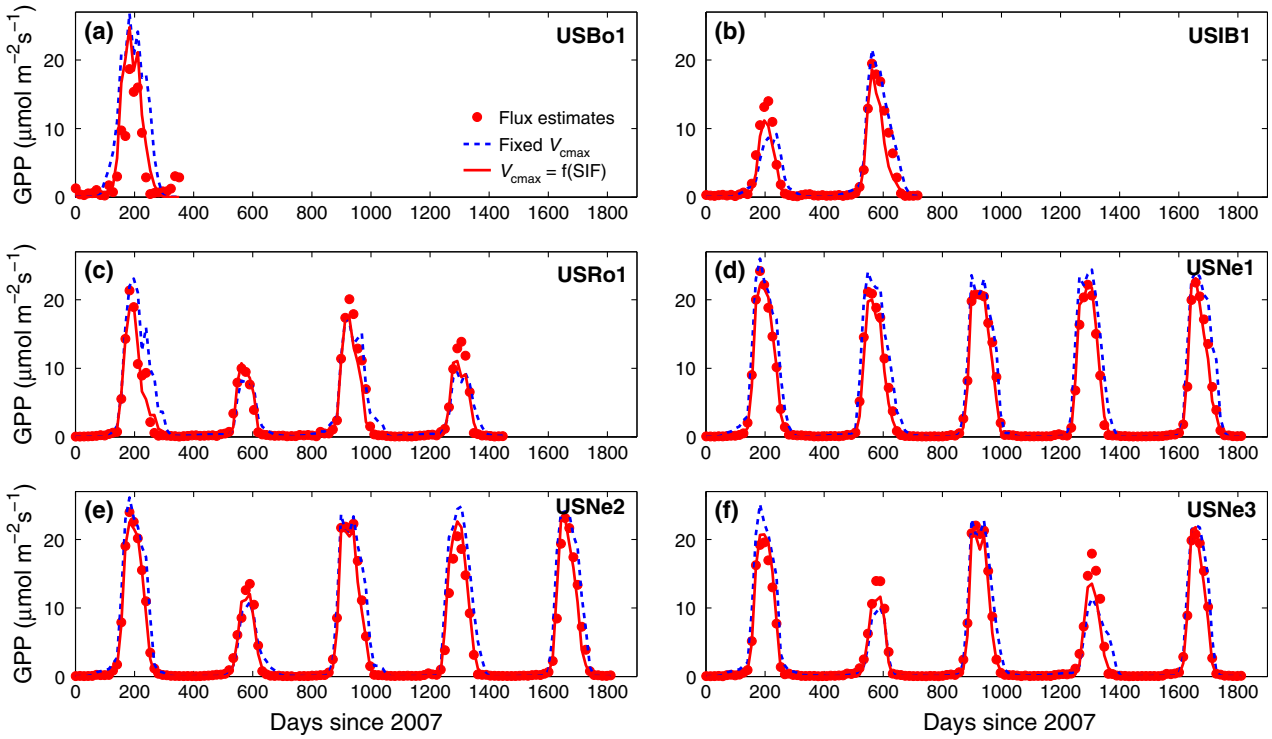


**Fig. 8** Seasonal variations of flux tower estimated gross primary productivity and Soil-Canopy Observation of Photosynthesis and Energy simulations with constant $V_{cmax}$ and seasonally varying $V_{cmax}$ at biweekly time steps for the six flux sites. (a)USBo1, (b)USIB1, (c)USRo1,(d)USNe1,(e)USNe2, and (f)USNe3. See Table 1 for site information.

are poor correlations between simulated and observed $LUE_p$ and $LUE_f$ and disagreement with the 1 : 1 line. After optimization with seasonally varying $V_{cmax}$ derived from SIF, the regression of observed vs. modeled $LUE_p$ and $LUE_f$ is closer to the 1 : 1 line (slopes of 0.93 and 1.28 for $LUE_p$ and $LUE_f$, respectively, in Figs 10 and 11). At site level, the mean bias error (MAE) is reduced from 0.54 to 0.36 and 0.15 to 0.08 $LUE_p$ and $LUE_f$, respectively, leading to a decrease in bias of 40% on average (Table 3).

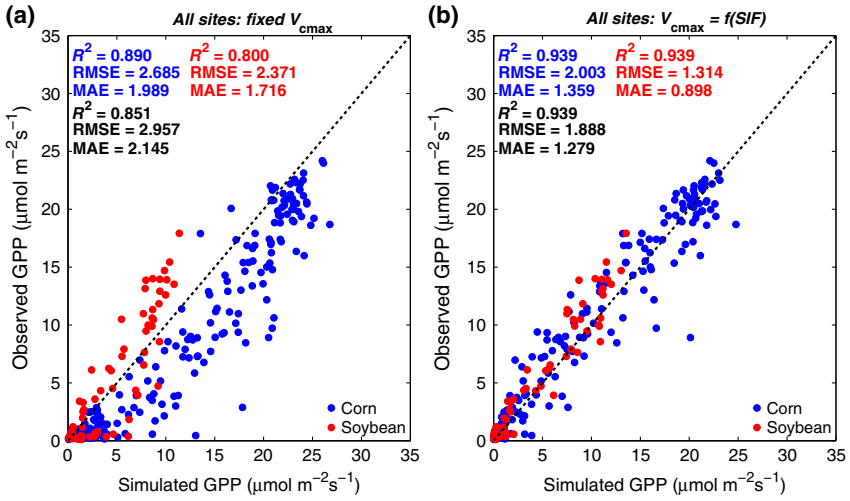


**Fig. 9** Scatter plots of flux tower estimated gross primary productivity against Soil-Canopy Observation of Photosynthesis and Energy simulations at a biweekly step with (a) constant $V_{cmax}$ and (b) seasonal variable $V_{cmax}$ at biweekly step during 2007–2011 for all sites.

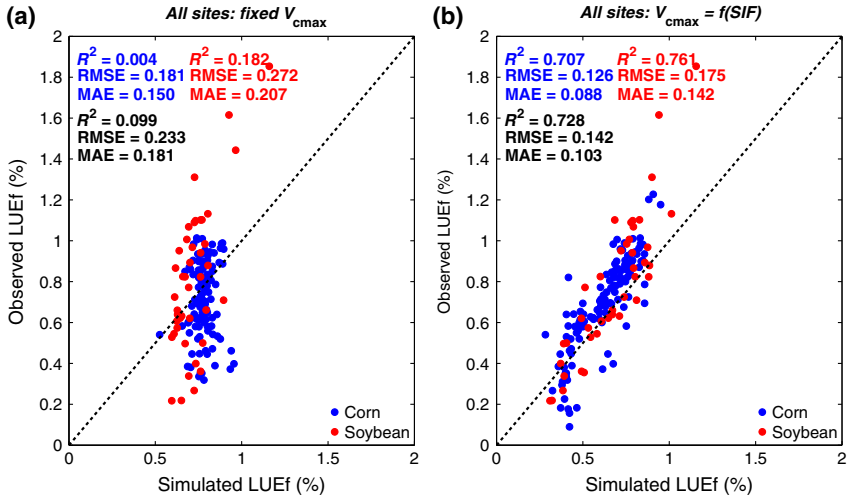


**Fig. 10** Scatter plots of flux tower estimated fluorescence yield ($LUE_f$) against Soil-Canopy Observation of Photosynthesis and Energy simulations at a biweekly time step during growing season with (a) constant $V_{cmax}$ and (b) seasonal variable $V_{cmax}$ for all site-years during 2007–2011.

## Discussion

Previous studies showed that chlorophyll fluorescence is a powerful technique to quantify photosynthetic efficiency and monitor vegetation dynamics (Flexas *et al.*, 2002; Meroni *et al.*, 2008; Damm *et al.*, 2010). With recent retrievals of SIF (Joiner *et al.*, 2013), Guanter *et al.* (2014) first showed the feasibility to monitor crop photosynthesis at regional to global scale, and capture the high photosynthetic rate of the corn belt of mid-western US. Following that work, our study shows that we are also able to derive sensible space-based estimates of seasonal $V_{cmax}$ by combining space-based retrievals of SIF and a photochemistry and radiative transfer model (SCOPE).

### *Comparison of obtained $V_{cmax}$ in corn and soybean with literature values*

In this study, the estimates of $V_{cmax}$ (Fig. 3) are within the range of those reported in the literature for corn and soybean except for several of the higher values (Wullschleger, 1993; Kattge & Knorr, 2007; Kattge *et al.*, 2009; Houborg *et al.*, 2013). Houborg *et al.* (2013), for example, reported $V_{cmax}$ at 25 °C of 11 to 48 μmol $m^{-2}$ $s^{-1}$ for corn during the growing season derived from leaf chlorophyll (Chl) content. For comparison, most of our estimations range from 11 to 64 μmol $m^{-2}$ $s^{-1}$ for $V_{cmax}$ of corn. For soybean, our retrieved values of $V_{cmax}$ are between 95 and 134 μmol $m^{-2}$ $s^{-1}$ during the mid-growing season, which is in good

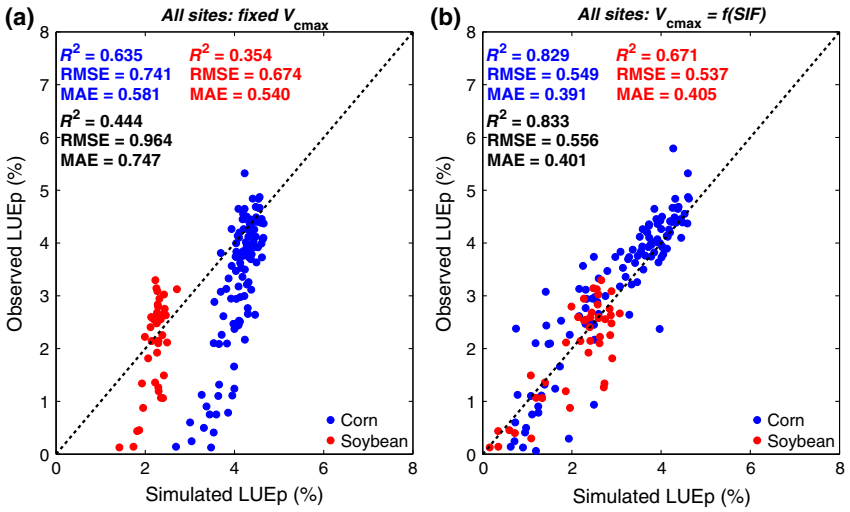


**Fig. 11** Scatter plots of flux tower measured light use efficiency of photosynthesis ($LUE_p$) against Soil-Canopy Observation of Photosynthesis and Energy simulations at biweekly step during the growing season with (a) constant $V_{cmax}$ and (b) seasonal variable $V_{cmax}$ at biweekly step for all site-years during 2007–2011.

agreement with field estimates from gas exchange measurements during mid-August near Champaign, IL, USA (Ainsworth *et al.*, 2014). They reported values of $V_{cmax}$ at 25 °C ranging from 76 to 136 μmol $m^{-2}$ $s^{-1}$ for soybean. On the other hand, we estimate slightly higher values of $V_{cmax}$ for soybean during the early growing season, varying between 160 and 190 μmol $m^{-2}$ $s^{-1}$. This larger $V_{cmax}$ during the early growing season may be due to two combined reasons: (1) larger slopes between $V_{cmax}$ and SIF due to this period being not Rubisco-limited (Fig. 3); and (2) spatial mismatch between GOME-2 pixel and flux tower footprint. This suggests the limitations that are primarily due to the current data availability of SIF. We assumed relatively homogeneous landscape for GOME-2 pixel, but there is obviously spatial variability within such a footprint, especially the mosaic of soybean and corn. In addition, there are different seasonal patterns of soybean and corn. As shown in Fig. 5, an earlier onset of the growing season was observed for soybean year through SIF from satellite while measurements were later from the flux tower. Hence, the assumption that it can be represented equally well for soybean and corn is tenuous in the early seasons (early to mid-June). The future retrievals of SIF with higher spatial resolution from the Sentinel-5 Precursor (TROPOMI, Veefkind *et al.*, 2012) would address this issue.

### *Effects of seasonal variability in $V_{cmax}$*

Including the seasonal patterns of $V_{cmax}$ in photosynthesis simulations significantly improved the agreement between independently modeled and measured estimates of GPP over the growing season for croplands (Figs 7–9). This result is in good agreement with other studies that found better modeling of $CO_2$ exchange between terrestrial ecosystems and the atmosphere by considering seasonal variations of $V_{cmax}$ (Wilson *et al.*, 2001; Houborg *et al.*, 2013; Medvigy *et al.*, 2013). In addition, the substantial improvements between modeled and flux tower derived estimates of $LUE_p$ and $LUE_f$ further increase our confidence that space retrievals of SIF can be used to invert seasonally varying $V_{cmax}$ and improve modeling of GPP and LUE (Figs 10 and 11). Assuming a constant value of $V_{cmax}$ in the simulations with SCOPE over the growing season results in overestimating GPP for corn but underestimating that for soybean. Yet, this approach of parameterizing $V_{cmax}$ with constant values is widely implemented in most of terrestrial biosphere models due to the difficulties of measuring in the field and to prescribe values on a global scale (Kattge *et al.*, 2009). This study addresses the need to consider seasonal variability in photosynthetic capacity for croplands and provides an approach to derive sensible space-based estimates of seasonal $V_{cmax}$ with space-based measurements of SIF.

### *Implications for biophysical models*

Our results suggest that measurements of SIF provide a new indicator of the magnitude and seasonality in $V_{cmax}$. Recently, spectroscopic data has been used to estimate various leaf or canopy-level biophysical parameters (Gillon *et al.*, 1999; Asner & Martin, 2008). However, there are only a few studies that have related

spectral data to photosynthetic capacity parameters ($V_{cmax}$) in the literature (Doughty *et al.*, 2011; Serbin *et al.*, 2011; Ainsworth *et al.*, 2014). In these studies, $V_{cmax}$ values were estimated for short-term periods using full-spectrum leaf optical properties from ground measurements. To our knowledge, there is only one other study that explored this potential relationship with satellite data (Houborg *et al.*, 2013), in which they quantified the seasonal variability in $V_{cmax}$ over a corn growing season based on Landsat-derived leaf chlorophyll estimates and a generalized indirect $V_{cmax}$ – Chl relationship for leaf nitrogen. On an operational basis, however, the required hyperspectral instruments are not currently available from space and satellite retrievals of Chl remain complex and uncertain. In this case, chlorophyll fluorescence, which has a much more direct link to vegetation photosynthetic activity, can provide an alternative way to more accurately assess key biophysical properties of vegetation compared to traditional reflectance-based measures.

The mechanistic relationship between SIF and $V_{cmax}$, shown in this study, offers the advantage of directly integrating SIF information into TBMs that rely on the C3 and C4 photosynthesis model developed by Farquhar *et al.* (1980) and Collatz *et al.* (1992). To more accurately quantify global and regional terrestrial GPP, information is needed on the seasonal variability of $V_{cmax}$ (Wilson *et al.*, 2001; Medvigy *et al.*, 2013). As Bonan *et al.* (2011) has pointed out, it is important to parameterize $V_{cmax}$ for simulating GPP because model structural errors can be partially compensated for by adjusting this parameter. In many modeling exercises, however, $V_{cmax}$ was assumed to be constant for each broadly defined PFT over time. It has long been sought to estimate the photosynthetic capacity of plant canopies from remote sensing data in space and time. The highly correlated relationship between $V_{cmax}$ and canopy-level chlorophyll fluorescence can be used to derive seasonal $V_{cmax}$ from space retrievals of SIF provided that other parameters, such as LAI and $C_{ab}$, are available from ancillary observations.

It should be pointed out that other parameters especially LAI may have similar effects to $V_{cmax}$ on the simulations of chlorophyll fluorescence. Systematic errors in LAI may lead to compensating errors in the inversion of $V_{cmax}$. In this study we have used *in situ* field measurements of LAI from the sites and hence this should not be important problem in our inversion of $V_{cmax}$. However, some sensitivity analyses need to be done in the future especially if LAI data is used from ancillary satellite-based measurements. Another point should be noted that, SCOPE is based on Collatz *et al.* (1991, 1992) for photosynthesis which assumes that the proximal cause of the decrease in photosynthetic capacity at elevated leaf temperature is incomplete activation of Rubisco. In the original Farquhar *et al.* model, this control is attributed to potential rate of electron transport ($J_{max}$). This parameter is used in several land surface models (e.g., CLM) and is generally assumed to be a constant ratio with $V_{cmax}$ across species (Wullschleger, 1993). Variations of this ratio have been found for different species (Medlyn *et al.*, 2002; Onoda *et al.*, 2005). However, we don't anticipate that this difference in model structure would have any significant effect on the inversions for $V_{cmax}$ reported here.

To conclude, we demonstrated that the magnitude and seasonal variability of $V_{cmax}$ can be estimated with chlorophyll fluorescence, and that the consideration of seasonally varying $V_{cmax}$ improves the modeling of GPP and LUE for both C3 and C4 crops. We evaluated the performance of our methods using six AmeriFlux eddy covariance flux sites in the midwestern US. A high correlation (linear relationship) was found between $V_{cmax}$ and SIF using SCOPE simulations for different vegetative growth stages during the growing season when other parameters in the model are specified using ancillary data. The resulting relationships were utilized to determine the magnitude and seasonal variability of $V_{cmax}$ from GOME-2 SIF retrievals at biweekly time steps. This study indicates that the use of seasonally varied $V_{cmax}$ derived from SIF, rather than a fixed PFT-specific value, significantly improves the agreement of simulated GPP and LUE with the observed tower fluxes.

Our approach provides the basis for regional or even global estimation of key photosynthetic capacity parameters like $V_{cmax}$ from the state-of-the-art remote sensing instruments. These estimates may represent a unique data for the constraint and benchmarking of TBMs in which global vegetation is typically classified by biome, and LUTs are used to estimate model parameters for each biome (Sellers *et al.*, 1997), especially for the key parameter of $V_{cmax}$. There are now two GOME-2 instruments on the MetOp-A and MetOp-B (launched in 2006 and 2013, respectively), and the MetOp-A is now providing data at a higher spatial resolution ($40 \times 40$ km$^2$). This will lead to improved fluorescence data sets for further studies. In addition, several future instruments, such as the Orbiting Carbon Observatory-2 (OCO-2) (Frankenberg *et al.*, 2014) and the Sentinel-5 Precursor (TROPOMI, Veefkind *et al.*, 2012) satellite missions to be launched in 2014–2016 will provide data with an up to 100-time improvement in spatial resolution and total number of observations. This will especially benefit the applications over the fragmented agricultural areas such as in Europe and China, and improve the application of our approach. With these

high spectral and spatial resolution instruments, we could have not only the ability to derive the seasonal variability of leaf photosynthetic capacity, but also the potential to map $V_{cmax}$ on a broad scale over fragmented areas. This would provide large-scale observations of $V_{cmax}$ that could further facilitate the parameterization improvements for the dynamic global vegetation models.

## Acknowledgements

We would like to thank the two reviewers for their valuable comments and suggestions. The work by YZ and LG has been funded by the Emmy Noether Programme (GlobFluo project) of the German Research Foundation. JJ was supported by the NASA Carbon Cycle Science program (NNH10DA001N). We acknowledge Eumetsat for the GOME-2 data. MODIS MOD13 EVI/NDVI data were obtained from the MODIS LP DAAC archive and MERIS-MTCI from the Infoterra Ltd server. This work used eddy covariance data acquired by AmeriFlux. We further thank PIs of the flux tower sites: T. Meyers (NOAA/ARL), D. Cook and R. Matamala (Argonne National Laboratory), and A. Suyker (Univ. Nebraska).

## Conflicts of interest

The authors declare no conflict of interest.

## References

Ainsworth EA, Serbin SP, Skoneczka JA *et al.* (2014) Using leaf optical properties to detect ozone effects on foliar biochemistry. *Photosynthesis Research*, **119**, 65–76.

Allison V J, Miller RM, Jastrow JD *et al.* (2004) Changes in soil microbial community structure in a tallgrass prairie chronosequence. *Soil Science Society of America Journal*, **69**, 1412–1421.

Asner GP, Martin RE (2008) Spectral and chemical analysis of tropical forests: scaling from leaf to canopy levels. *Remote Sensing of Environment*, **112**, 3958–3970.

Baker NR (2008) Chlorophyll fluorescence: a probe of photosynthesis in vivo. *Annual Reviews – Plant Biology*, **59**, 89–113.

Ball JT, Woodrow IE, Berry JA (1991) *A Model Predicting Stomatal Conductance and Its Contribution to the Control of Photosynthesis under Different Environmental Conditions. Progress in Photosynthesis Research*. Springer, the Netherlands, pp. 221–224.

Bauerle WL, Oren R, Way DA *et al.* (2012) Photoperiodic regulation of the seasonal pattern of photosynthetic capacity and the implications for carbon cycling. *Proceedings of the National Academy of Sciences of the United States of America*, **109**, 8612–8617.

Bonan GB, Lawrence PJ, Oleson KW *et al.* (2011) Improving canopy processes in the Community Land Model version 4 (CLM4) using global flux fields empirically inferred from FLUXNET data. *Journal of Geophysical Research*, **116**, G02014.

von Caemmerer S, Farquhar GD (1981) Some relationships between the biochemistry of photosynthesis and the gas exchange of leaves. *Planta*, **153**, 376–387.

Collatz GJ, Ball JT, Grivet C, Berry JA (1991) Physiological and environmental regulation of stomatal conductance, photosynthesis and transpiration: a model that includes a laminar boundary layer. *Agricultural and Forest Meteorology*, **54**, 107–136.

Collatz GJ, Ribas-Carbo M, Berry JA (1992) Coupled photosynthesis-stomatal conductance model for leaves of C4 plants. *Australian Journal of Plant Physiology*, **19**, 519–538.

Combal B, Baret F, Weiss M *et al.* (2003) Retrieval of canopy biophysical variables from bidirectional reflectance: using prior information to solve the ill-posed inverse problem. *Remote Sensing of Environment*, **84** , 1–15.

Damm A, Elbers J, Erler A *et al.* (2010) Remote sensing of sun-induced fluorescence to improve modeling of diurnal courses of gross primary production (GPP). *Global Change Biology*, **16**, 171–186.

Darvishzadeh RA, Skidmore M, Schlerf C *et al.* (2008) Inversion of a radiative transfer model for estimating vegetation LAI and chlorophyll in a heterogeneous grassland. *Remote Sensing of Environment*, **112** , 2592–2604.

Dash J, Curran PJ (2004) The MERIS terrestrial chlorophyll index. *International Journal of Remote Sensing*, **25**, 5403–5413.

Dickinson RE (1983) Land surface processes and climate surface albedos and energybalance. *Advances in Geophysics*, **25**, 305–353.

Doughty C, Asner G, Martin R (2011) Predicting tropical plant physiology from leaf and canopy spectroscopy. *Oecologia*, **165**, 289–299.

Edwards GE, Baker NR (1993) Can $CO_2$ assimilation in maize leaves be predicted accurately from chlorophyll fluorescence analysis? *Photosynthesis Research*, **37**, 89–102.

Farquhar GD, von Caemmerer S, Berry JA (1980) A biochemical model of photosynthetic $CO_2$ assimilation in leaves of C3 species. *Planta*, **149**, 78–90.

Flexas J, Escalona JM, Evain S *et al.* (2002) Steady-state chlorophyll fluorescence (FS) measurements as a tool to follow variations of net $CO_2$ assimilation and stomatal conductance during water-stress in C3 plants. *Physiologia Plantarum*, **114**, 231–240.

Frankenberg C, Fisher JB, Worden J *et al.* (2011) New global observations of the terrestrial carbon cycle from GOSAT: patterns of plant fluorescence with gross primary productivity. *Geophysical Research Letter*, **38**, L17706.

Frankenberg C, O'Dell C, Berry JA *et al.* (2014) Prospects for chlorophyll fluorescence remote sensing from the Orbiting Carbon Observatory-2. *Remote Sensing of Environment*, **147**, 1–12.

Friedl MA, Sulla-Menashe D, Tan B *et al.* (2010) MODIS collection 5 global land cover: algorithm refinements and characterization of new datasets. *Remote Sensing of Environment*, **114** , 168–182.

Genty B, Briantais J-M, Baker NR (1989) The relationship between the quantum yield of photosynthetic electron transport and quenching of chlorophyll fluorescence. *Biochimica et Biophysica Acta*, **990**, 87–92.

Gillon D, Houssard C, Joffrey R (1999) Using near-infrared reflectance spectroscopy to predict carbon, nitrogen and phosphorus content in heterogeneous plant material. *Oecologia*, **118**, 173–182.

Gitelson AA, Peng Y, Masek JG *et al.* (2012) Remote estimation of crop gross primary production with Landsat data. *Remote Sensing of Environment*, **121**, 404–414.

Govindjee (2004) Chlorophyll a fluorescence: a bit of basics and history. In: *Chlorophyll A Fluorescence: A Signature of Photosynthesis. Advances in Photosynthesis and Respiration*, Vol. 19 (eds Papageorgiou GC, Govindjee), pp. 1–42. Springer, Dordrecht.

Grassi G, Vicinelli E, Ponti F *et al.* (2005) Seasonal and interannual variability of photosynthetic capacity in relation to leaf nitrogen in a deciduous forest plantation in northern Italy. *Tree Physiology*, **25**, 349–360.

Griffis TJ, Sargent SD, Baker JM *et al.* (2008) Direct measurement of biosphere-atmosphere isotopic $CO_2$ exchange using the eddy covariance technique. *Journal of Geophysical Research: Atmospheres*, **113**, D08304, doi: 10.1029/2007JD009297.

Guanter L, Frankenberg C, Dudhia A *et al.* (2012) Retrieval and global assessment of terrestrial chlorophyll fluorescence from GOSAT space measurements. *Remote Sensing of Environment*, **121**, 236–251.

Guanter L, Zhang Y, Jung M *et al.* (2014) Global and time-resolved monitoring of crop photosynthesis with chlorophyll fluorescence. *Proceedings of the National Academy of Sciences of the United States of America*, **111**, E1327–E1333.

Hanson PJ, Amthor JS, Wullschleger SD *et al.* (2004) Oak forest carbon and water simulations: model intercomparisons and evaluations against independent data. *Ecological Monographs*, **74**, 443–489.

Hilker T, Coops NC, Wulder MA *et al.* (2008) The use of remote sensing in light use efficiency based models of gross primary production: a review of current status and future requirements. *Science of the Total Environment*, **404**, 411–423.

Hilker T, Coops NC, Hall FG *et al.* (2011) Inferring terrestrial photosynthetic light use efficiency of temperate ecosystems from space. *Journal of Geophysical Research: Biogeosciences*, **116**, G03014. doi: 10.1029/2011JG001692.

Hosgood B, Jacquemoud S, Andreoli G *et al.* (1994) *Leaf Optical Properties EXperiment 93 (LOPEX93)*. European Commission – Joint Research Centre, Ispra, Italy. EUR 16095 EN.

Houborg R, Cescatti A, Migliavacca M *et al.* (2013) Satellite retrievals of leaf chlorophyll and photosynthetic capacity for improved modeling of GPP. *Agricultural and Forest Meteorology*, **177**, 10–23.

Huete AR, Didan K, Miura T *et al.* (2002) Overview of the radiometric and biophysical performance of the MODIS vegetation indices. *Remote Sensing of Environment*, **83**, 195–213.

Jacquemoud S, Baret F (1990) PROSPECT: a model of leaf optical properties spectra. *Remote Sensing of Environment*, **34**, 75–91.

Jacquemoud S, Ustin SL, Verdebout J *et al.* (1996) Estimating leaf biochemistry using the PROSPECT leaf optical properties model. *Remote Sensing of Environment*, **56**, 194–202.

Joiner J, Yoshida Y, Vasilkov AP *et al.* (2011) First observations of global and seasonal terrestrial chlorophyll fluorescence from space. *Biogeosciences*, **8** , 637–651.

Joiner J, Yoshida Y, Vasilkov AP *et al.* (2012) Filling-in of near-infrared solar lines by terrestrial fluorescence and other geophysical effects: simulations and space-based observations from SCIAMACHY and GOSAT. *Atmospheric Measurement Techniques*, **5**, 809–829.

Joiner J, Guanter L, Lindstrot R *et al.* (2013) Global monitoring of terrestrial chlorophyll fluorescence from moderate-spectral-resolution near-infrared satellite measurements: methodology, simulations, and application to GOME-2. *Atmospheric Measurement Techniques*, **6**, 2803–2823.

Kattge J, Knorr W (2007) The temperature dependence of photosynthetic capacity in a photosynthesis model acclimates to plant growth temperature: a re-analysis of data from 36 species. *Plant Cell and Environment*, **30**, 1176–1190.

Kattge J, Knorr W, Raddatz T *et al.* (2009) Quantifying photosynthetic capacity and its relationship to leaf nitrogen content for global scale terrestrial biosphere models. *Global Change Biology*, **15**, 976–991.

Kosugi Y, Shibata S, Kobashi S (2003) Parameterization of the $CO_2$ and $H_2O$ gas exchange of several temperate deciduous broad-leaved trees at the leaf scale considering seasonal changes. *Plant Cell and Environment*, **26**, 285–301.

Lemeur R, Blad BL (1974) A critical review of light models for estimating the shortwave radiation regime of plant canopies. *Agricultural Meteorology*, **14** , 5–286.

Lokupitiya E, Denning S, Paustian K *et al.* (2009) Incorporation of crop phenology in simple biosphere model (sibcrop) to improve land-atmosphere carbon exchanges from croplands. *Biogeosciences*, **6**, 969–986.

Maire GL, François C, Dufrêne E (2004) Towards universal deciduous broad leaf chlorophyll indices using PROSPECT simulated database and hyperspectral reflectance measurements. *Remote Sensing of Environment*, **89**, 1–28.

Mäkelä A, Hari P, Berninger F *et al.* (2004) Acclimation of photosyn-thetic capacity in Scots pine to the annual cycle of temperature. *Tree Physiology*, **24**, 369–376.

Medlyn BE, Dreyer E, Ellsworth D *et al.* (2002) Temperature response of parameters of a biochemically based model of photosynthesis. II. A review of experimental data. *Plant, Cell and Environment*, **25**, 1167–1179.

Medvigy D, Wofsy SC, Munger JW *et al.* (2009) Mechanistic scaling of ecosystem function and dynamics in space and time: ecosystem demography model version 2. *Journal of Geophysical Research*, **114**, G01002.

Medvigy D, Jeong S-J, Clark KL (2013) Effects of seasonal variation of photosynthetic capacity on the carbon fluxes of a temperate deciduous forest. *Journal of Geophysical Research: Biogeosciences*, **118**, 1703–1714.

Meroni M, Rossini M, Picchi V *et al.* (2008) Assessing steady-state fluorescence and PRI from hyperspectral proximal sensing as early indicators of plant stress: the case of ozone exposure. *Sensors*, **8**, 1740–1754.

Miller J, Berger M, Goulas Y *et al.* (2005) Development of a Vegetation Fluorescence Canopy Model. ESTEC Contract No. 16365/02/NL/FF, Final Report, 138 pp.

Oleson KW, Lawrence DM, Bonan GB *et al.* (2010) *Technical Description of Version 4.0 of the Community Land Model (CLM)*. NCAR Technical Note NCAR/TN-478 + STR. NCAR, Boulder, CO.

Onoda Y, Hikosaka K, Hirose T (2005) The balance between RuBP carboxylation and RuBP regeneration: a mechanism underlying the interspecific variation in acclimation of photosynthesis to seasonal change in temperature. *Functional Plant Biology*, **32**, 903–910.

Papale D, Reichstein M, Aubinet M *et al.* (2006) Towards a standardized processing of Net Ecosystem Exchange measured with eddy covariance technique: algorithms and uncertainty estimation. *Biogeosciences*, **3**, 571–583.

Reichstein M, Falge E, Baldocchi D *et al.* (2005) On the separation of net ecosystem exchange into assimilation and ecosystem respiration: review and improved algorithm. *Global Change Biology*, **11**, 1424–1439.

Running SW, Nemani RR, Heinsch FA *et al.* (2004) A continuous satellite-derived measure of global terrestrial primary production. *BioScience*, **54**, 547–560.

Ryu Y, Baldocchi DD, Black TA *et al.* (2011) On the temporal upscaling of evapotranspiration from instantaneous remote sensing measurements to 8-day mean daily-sums. *Agricultural and Forest Meteorology*, **152**, 212–222

Schaefer K, Schwalm CR, Williams C *et al.* (2012) A model-data comparison of gross primary productivity: results from the North American Carbon Program site synthesis. *Journal of Geophysical Research*, **117**, G03010.

Sellers PJ, Berry JA, Collatz GJ *et al.* (1992) Canopy reflectance, photosynthesis, and transpiration. III. A reanalysis using improved leaf models and a new canopy integration scheme. *Remote Sensing of Environment*, **42** , 187–216.

Sellers PJ, Dickinson RE, Randall DA *et al.* (1997) Modeling the exchanges of energy, water, and carbon between continents and the atmosphere. *Science*, **275** , 502–509.

Serbin SP, Dillaway DN, Kruger EL *et al.* (2011) Leaf optical properties reflect variation in photosynthetic metabolism and its sensitivity to temperature. *Journal of Experimental Botany*, **63** , 489–502.

Suyker AE, Verma SB, Burba GG *et al.* (2005) Gross primary production and ecosystem respiration of irrigated maize and irrigated soybean during a growing season. *Agricultural and Forest Meteorology*, **131**, 180–190.

van der Tol C, Verhoef W, Timmermans J *et al.* (2009a) An integrated model of soil-canopy spectral radiances, photosynthesis, fluorescence, temperature and energy balance. *Biogeosciences*, **6**, 3109–3129.

van der Tol C, Verhoef W, Rosema A (2009b) A model for chlorophyll fluorescence and photosynthesis at leaf scale. *Agricultural and Forest Meteorology*, **149** , 96–105.

Tucker CJ (1979) Red and photographic infrared linear combinations for monitoring vegetation. *Remote Sensing of Environment*, **8** , 127–150.

Turner DP, Urbanski S, Bremer D *et al.* (2003) A cross-biome comparison of daily light use efficiency for gross primary production. *Global Change Biology*, **9**, 383–395.

USDA (2010) *Field Crops – Usual Planting and Harvesting Dates. Agricultural Handbook Number 628*. United States Department of Agriculture, National Agricultural Statistics Service, Washington, DC.

USDA National Agricultural Statistics Service Cropland Data Layer (2013) *Published Crop-specific Data Layer* [Online]. USDA-NASS, Washington, DC. Available at: http://nassgeodata.gmu.edu/CropScape/(accessed 15 December 2013).

Veefkind JP, Aben I, McMulla K *et al.* (2012) TROPOMI on the ESA Sentinel-5 Precursor: a GMES mission for global observations of the atmospheric composition for climate, air quality and ozone layer applications. *Remote Sensing of Environment*, **120**, 70–83.

Verhoef W, Bach H (2007) Coupled soil-leaf-canopy and atmosphere radiative transfer modeling to simulate hyperspectral multi-angular surface reflectance and TOA radiance data. *Remote Sensing of Environment*, **109**, 166–182.

Wang YP, Baldocchi DD, Leuning R *et al.* (2007) Estimating parameters in a land-surface model by applying nonlinear inversion to eddy covariance flux measurements from eight FLUXNET sites. *Global Change Biology*, **13**, 652–670.

Weis E, Berry JA (1987) Quantum efficiency of photosystem II in relation to 'energy'-dependent quenching of chlorophyll fluorescence. *Biochimica et Biophysica Acta*, **894**, 198–208.

Wilson KB, Baldocchi DD, Hanson PJ (2001) Leaf age affects the seasonal pattern of photosynthetic capacity and net ecosystem exchange of carbon in a deciduous forest. *Plant Cell Environment*, **24**, 571–583.

Wolf A, Akshalov K, Saliendra N *et al.* (2006) Inverse estimation of Vcmax, leaf area index, and the Ball-Berry parameter from carbon and energy fluxes. *Journal of Geophysical Research*, **111**, D08S08.

Wullschleger SD (1993) Biochemical limitations to carbon assimilation in C3 plants – a retrospective analysis of the A/Ci curves from 109 species. *Journal of Experimental Botany*, **44** , 1993.

Xu L, Baldocchi DD (2003) Seasonal trends in photosynthetic parameters and stomatal conductance of blue oak (Quercus douglasii) under prolonged summer drought and high temperature. *Tree Physiology*, **23**, 865–877.